TriDurLE

National Center for Transportation Infrastructure Durability & Life-Extension

Project ID: 2020-UU-01

PERFORMANCE OF ABC COLUMNS AND COST-EFFECTIVE RETROFIT STRATEGIES SUBJECTED TO SYNERGISTIC DISTRESS RESULTING FROM CORROSION AND SEISMIC LOADING: PART II

Chris P. Pantelides

Sayal Shrestha

University National Transportation Center TriDurLE

Department of Civil and Environmental Engineering

405 Spokane Street PO Box 642910

Washington State University Pullman, WA 99164-2910

June 2024

ACKNOWLEDGEMENTS

The authors acknowledge the grant provided by the TriDurLE National Transportation Center. The authors would also like to acknowledge Duc Tranquang of the University of Utah for his assistance in the conceptual stage of the experiments. The authors would like to thank Mark Bryant, Ijan Dangol, Duc Tranquang, Dylan Briggs, Suman Neupane and Emily Williamson for their help in the process of building and testing the specimens.

DISCLAIMER

The authors alone are responsible for the preparation and accuracy of the information, data, analysis, discussions, recommendations, and conclusions presented. The contents do not necessarily reflect the views, opinions, endorsements, or policies of the TriDurLE National Transportation Center which makes no representation or warranty of any kind and assumes no liability, therefore.

TABLE OF CONTENTS

LIST OF FIGURES

LIST OF TABLES

EXECUTIVE SUMMARY

Accelerated Bridge Construction (ABC) is a novel bridge construction method that saves construction time. Over the lifespan of a bridge, columns in bridges built with ABC methods are vulnerable to corrosion, which adversely influences bridge performance during earthquakes. Post-tensioned (PT) bars are used in precast concrete columns to reduce residual drift after an earthquake. The effects of corrosion on concrete bridge columns reinforced with two longitudinal unbonded PT bars and steel or glass fiber-reinforced polymer (GFRP) spiral bars are studied. Four specimens were constructed with the two types of spiral reinforcement used for confinement: (i) two constructed with a steel spiral and (ii) two constructed with a GFRP spiral; this was done to observe whether the spiral material can influence the corrosion rate of longitudinal steel reinforcement and the influence of corrosion on the seismic performance of the columns. One specimen with each spiral material was tested without any imposed corrosion as the control specimen. The second specimen of each spiral material type was placed through an accelerated corrosion process for 114 days; this was the time taken to achieve significant corrosion in a similar study by the authors for specimens of similar dimension but with different details of reinforcement. Quasi-static cyclic tests were subsequently performed on all the specimens to obtain the hysteretic response of the columns. The research outlines the difference in the seismic performance of the control and corroded columns. Additionally, the research studies the difference in the amount of corrosion of longitudinal steel bars when steel spiral or a GFRP spiral is used to reinforce precast concrete columns. Finally, the seismic performance of a fifth specimen is presented for a corroded reinforced concrete column constructed with ABC methods, which was repaired with a carbon fiber-reinforced polymer (CFRP) shell and vertical headed steel bars.

1 INTRODUCTION

Accelerated Bridge Construction (ABC) is a novel method of construction that has many advantages over traditionally constructed cast-in-place (CIP) bridges (Ameli et al. 2015). Using the ABC method in urban areas decreases bridge building time and improves construction quality (Culmo 2011). Reinforced concrete (RC) bridges built through ABC methods must endure the same environmental conditions as CIP bridges throughout their lifespan. Consequently, they are susceptible to corrosion of steel reinforcing bars caused by de-icing salts in cold regions and exposure to salt water in marine environments. Moreover, these bridges are designed to resume functionality immediately after an earthquake. To achieve this objective, post-tensioned (PT) bars are used to minimize the residual drift of the columns (Dangol and Pantelides 2022; Neupane and Pantelides 2024). Corrosion of longitudinal steel reinforcement may cause PT bars to be stressed differently, potentially causing the seismic response of the column to change. Therefore, the seismic performance of corroded concrete columns in bridges built using ABC methods reinforced with PT bars is studied. In addition, a repair method for corroded reinforced concrete bridge columns constructed using ABC methods is presented.

1.1 PROBLEM STATEMENT

Although Accelerated Bridge Construction (ABC) methods are promising, there are challenges in their implementation that require further research. These challenges include an insufficient understanding of physical behavior, a lack of practice guidelines and specifications, cost-benefit analyses, and the time-dependent response of discrete members fabricated on-site or off-site. The seismic performance and long-term durability of bridges constructed using ABC methods remain largely unknown. As a result, practitioners and government engineers face difficulties when implementing ABC methods.

The ABC design manual from the Federal Highway Administration (FHWA) provides recommendations for the durability of prefabricated members and their connections (FHWA 2013). However, issues related to moisture ingress and deterioration remain unresolved. Another FHWA document presents case studies highlighting typical problems such as premature cracking and water leakage, which affect the performance

of installed ABC elements (FHWA 2013)

Corrosion is a significant problem in highway bridges, reducing the cross-sectional area of reinforcing steel, compromising structural integrity (e.g., concrete cracking and spalling), and diminishing the load-carrying capacity of the system. A recent survey reports that the direct cost of corrosion in the U.S. exceeds $500 billion (Akhoondan and Bell 2016). Existing structures often suffer from corrosion damage, leading to performance degradation below the intended design level. However, thorough investigations into the occurrence of steel corrosion and its implications for the seismic performance of ABC bridge elements have not yet been conducted, particularly for substructures frequently exposed to water and salt spray from de-icing salts.

Earthquake-induced loading is highly complex and can lead to catastrophic failures. Consequently, extensive research has focused on various aspects, such as seismic demand, ductility, stress variation, and the development of design requirements (Goodyear D. and Lund H. 2019). Regarding performance-based seismic bridge design, NCHRP Report 440 compiles relevant research (Marsh and Stringer 2013). Despite the significant impact of seismic loading, little is known about the seismic behavior of corrosion-damaged Accelerated Bridge Construction (ABC) elements in earthquake-prone zones. It remains unclear whether ABC systems are as vulnerable as conventional bridge systems when subjected to combined stresses from corrosion and seismic loading. Therefore, a study is necessary to elucidate the deterioration mechanisms of ABC bridge members and to develop comprehensive modeling and design guidelines for practitioners, as well as seismic repair and retrofit methods.

1.1 OBJECTIVES

The goal of this research is to enhance the durability and seismic performance of concrete columns in bridges constructed with ABC methods. Experimental programs alongside advanced modeling techniques are conducted:

i. to study the deterioration mechanisms of ABC bridge columns with PT bars and steel spiral reinforcement exposed to synergistic distress comprising corrosion and seismic loading,

ii. to study the deterioration mechanisms of ABC bridge columns with PT bars and GFRP spiral

reinforcement exposed to synergistic distress comprising corrosion and seismic loading,

iii. to compare the seismic performance of the corroded columns constructed using steel spiral and GFRP spiral, and

iv. to determine the seismic performance of repaired corroded reinforced concrete columns constructed with ABC methods.

1.2 EXPECTED CONTRIBUTIONS

The research is expected to contribute to the body of knowledge as follows:

i. fundamental knowledge of corrosion effects on seismic response of concrete bridge columns with PT bars constructed with ABC methods using steel or GFRP spiral reinforcements.

ii. performance of repaired corroded concrete columns constructed with ABC methods.

1.3 .REPORT OVERVIEW

The sequence of tasks required to carry out the research is outlined in this report. In addition, the report provides information about the relevant research tools. The following information is provided:

Chapter 1 provides an introduction and an overview of the problem statement, the objectives, and expected contributions.

Chapter 2 describes an overview of the literature on the effects of corrosion on reinforced concrete columns.

Chapter 3 describes the design, details, and construction process of the test specimens using ABC methods and the method used to simulate corrosion in the laboratory.

Chapter 4 includes the experimental findings of this report.

Chapter 5 includes a summary of this report and the conclusions.

2 LITERATURE REVIEW

2.1 EFFECTS OF CORROSION ON RC COLUMNS

Previous studies regarding corrosion of RC columns show that corrosion of steel reinforcement leads to a significant reduction in seismic performance (Apostolopoulos et al. 2019; Rodriguez et al. 1997). The reduction in performance is mainly attributed to cracking of the confined concrete core, the reduction in steel reinforcement, and loss of confining pressure (Campione et al. 2015). A study involving the seismic behavior of corroded RC columns under lateral seismic loads has been presented (Fang et al. 2017), corrosion significantly influencing the yield strength and ultimate load-bearing capacity of the column piers.

Corrosion of steel reinforcement causes cracking of concrete and loss of bond strength. The corrosion rust byproducts have a volume greater than that of the original steel bars; this causes an increase in volume inside the concrete, which develops tensile stresses that lead to cracking and spalling of the cover concrete (Ahmad 2003). Concrete cracks cause corrosive chemicals to seep deeper into the RC column, further corroding the steel reinforcement (Alonso et al. 1998; Fang et al. 2004).

There is a loss in the net area of reinforcing steel bars, which reduces their axial load-carrying capacity, leading to buckling of steel bars when an axial load is applied to the columns (Rodriguez et al. 1997). In addition, the cracking of concrete and corrosion of confining steel reinforcement can cause a reduction in the support of the vertical bars, leading to longer lengths of unsupported longitudinal bars, which causes buckling (Tapan and Aboutaha 2011).

Corrosion can lead to damage of the confining steel reinforcement such as spirals or stirrups. The confining steel reinforcement is designed to provide ductility in regions where plastic hinges could form in RC columns; thus, the confining steel reinforcement may become inadequate in corroded columns (Rajput and Sharma 2018). Corrosion of stirrups can reduce their confining ability and frictional bond stress; this can lead to loss of bond between corroded steel bars and the surrounding concrete. In addition, damage in the grip of steel bars causes a significant reduction of bond strength between the bars and concrete (Lin et

al. 2019); this poses a problem in structural components, specifically bridge columns, where loss of strength can cause bridge collapse in large earthquakes.

Reduction factors developed for steel bars that are used to estimate the residual capacity of corroded RC structures are not able to capture the reduction that occurs in real corroded RC columns and could lead to unsafe predictions of residual capacity (Andisheh et al. 2019). Fiber-reinforced polymer (FRP) wraps are used to recover the strength of RC columns affected by corrosion due to the high strength-to-weight ratio of the FRP composite and corrosion resistance (ACI 2017; Jia et al. 2020; Zhou et al. 2020) The use of PT bars increases the axial forces in the column. Using carbon-FRP (CFRP) sheets to wrap a column increases the axial strength and strain capacity of the column (Wang et al. 2012). The confinement provided by the CFRP jacket significantly affects the confined strength and ultimate strain of reinforced concrete columns (Saenz and Pantelides, 2006; Zhou et al., 2019). Soudki et al. (2007) showed a decrease in the corrosion rate of steel reinforcement in beamsrapped by CFRP jackets (Soudki et al. 2007). Similarly, Bae and Belarbi (2009) extended the finding by demonstrating a reduction in corrosion rate of steel reinforcement in columns under the protective wrapping of CFRP jackets (Bae and Belarbi 2009). However, corrosion was not stopped completely, and this resulted in the loss of ultimate axial compression capacity after the column was corroded.

2.2 GFRP SPIRALS TO REDUCE CORROSION

Glass-FRP (GFRP) spirals have been used in place of steel spirals in locations where corrosion of steel spirals was expected. A larger GFRP spiral needs to be used in place of the steel spiral to get similar confinement performance (Pantelides et al. 2013). In extensive column tests, it has been observed that GFRP spirals effectively confine the core concrete until the GFRP spirals reach failure. This leads to strain levels significantly surpassing the yield strain of steel (Kharal and Sheikh, 2020). Zhou et al. (2018) show that GFRP spirals can provide confinement to the columns even under exposure to high chloride levels for an extended period (Zhou et al. 2018). GFRP spirals can match or increase column ductility and displacement capacity compared to a column with steel spirals (Ali and El-Salakawy 2016; Kharal et al. 2021). Wright and Pantelides (2021a, 2021b) assessed concrete column performance under axial

compression, utilizing various non-corroding reinforcing materials. They found that the mass loss due to corrosion was notably lower at 7.0% for specimens reinforced with GFRP spiral, in stark contrast to a mass loss between 16.0% and 18.0% observed in columns with steel spirals (Wright and Pantelides 2021a; b).

2.3 RESIDUAL DRIFT AFTER EARTHQUAKE

Residual drift is a significant parameter to determine if a bridge can be used after an earthquake (Mackie and Stojadinovic 2004) The Japanese Road Association, following a thorough assessment of RC column behavior in the standing buildings after the 1995 Kobe earthquake has established a permissible residual drift ratio of 1.0%. (Kazuhiko 1997). PT bars have been used to reduce the residual drift of columns in seismically active zones (Ou et al. 2010; Sideris et al. 2014). Hybrid bridge bents with columns reinforced with PT bars can significantly reduced residual drift (Dangol and Pantelides 2022; Neupane and Pantelides 2024).

Many studies have been conducted on the effect of corrosion on the seismic performance of RC bridge columns (Basdeki et al. 2022; Choine M. N. 2014). The seismic performance of RC columns using PT bars for self-centering has been studied for conventional CIP-built columns (Palermo et al. 2007) and precast columns (Billington and Yoon 2004; Sideris et al. 2014). There have been few studies on the effects of steel reinforcement corrosion on the seismic performance of bridges built using ABC (Shrestha and Pantelides 2024a; b; Wang et al. 2021; Yuan et al. 2018). Research on the influence of corroded reinforcement in the seismic performance of bridge columns built using ABC is few, particularly those using PT bars for self-centering, is non-existent.

2.4 REPAIR OF COLUMN USING CFRP SHELL

Repair of corroded columns could restore their original strength and displacement capacity. Several methods exist for improving the strength of reinforced concrete (RC) columns affected by corrosion, one of which is fiber-reinforced polymer (FRP) composites (Jia et al. 2020; Zhou et al. 2020). Carbon-FRP (CFRP) composites have high strength-to-weight ratio and resist corrosion and fatigue stress (Gergely et al. 2000). CFRP sheets can be used as RC column jackets to confine the concrete and increase axial strength

and axial strain capacity (Pantelides et al. 1999; Wang et al. 2012). RC columns wrapped with CFRP jackets demonstrate negligible strength and ductility loss when subjected to subsequent corrosion after repair (Bae and Belarbi 2009; Tastani and Pantazopoulou 2004). However, it is not recommended to retrofit precast RC columns that have severe corrosion damage using CFRP jackets (Jia et al. 2020; Wang et al. 2021). Instead, a repair method using a CFRP shell, larger than the column diameter with headed steel bars epoxied inside the footing and concrete between the original column and the CFRP shell, is utilized in this research. This method has been used to repair precast concrete columns connected to footings with splice sleeve connectors (Parks et al. 2016). The repair method was further developed by adding a steel collar with studs inside the CFRP shell to increase bond between the column and repair concrete that restored the column's lateral force and displacement capacity A CFRP shell repair of corroded columns with headed steel bars and a steel collar is developed in this research.

3 METHODOLOGY

3.1 DESIGN OF SPECIMENS

Five specimens were constructed in this study using ABD methods. Four specimens had columns reinforced with PT bars, and one specimen without any PT bars (Shrestha and Pantelides 2024a; b). The four post-tensioned specimens had steel longitudinal bars but different types of spiral reinforcement: (a) two were constructed with a steel spiral, referred to as AS; and (b) two were constructed with a GFRP spiral, referred to as HYB. One of each type of column was put through an accelerated corrosion process for 114 days. The time of 114 days was chosen as the time taken for a reinforced concrete column without post-tensioning bars to be severely corroded or have a 25% mass loss of longitudinal steel (Shrestha and Pantelides 2024a). The columns and footing were cast separately and joined using a grouted duct method. After casting, Polyvinyl chloride (PVC) pipes were placed in the column and footing to accommodate the PT bars. The fifth specimen was constructed with steel longitudinal bars and a steel spiral; it also went through the accelerated corrosion process for 114 days. It was subsequently repaired with a CFRP shell and headed steel bars and tested under cyclic loads.

3.1.1 COLUMN DESIGN

The four post-tensioned specimens were designed as 38% scale models of highway bridges with grouted ducts used to connect the column to the footing (Shrestha and Pantelides 2024a), as shown in Fig. 1. The AASTHO LFRD Bridge Design Specifications (2012) and the AASHTO Guide Specifications for LFRD Seismic Bridge Design (2011) were used for the capacity-based seismic design of the specimens. An octagonal cross-sectional shape was chosen for ease of storage, transportation, and handling of the columns after casting. The initial design was performed for a CIP bridge for seismic zones C and D. Subsequent modifications were made to accommodate the grouted ducts and PT bars. The longitudinal bars were also intentionally debonded for large strain development and increased displacement ductility (Ameli et al. 2015; Tazarv and Saiidi 2015). The longitudinal reinforcing bars were debonded for 203 mm (8.0 in.) inside the column and 102 mm (4.0 in) inside the footing. The concrete mix design for a target compressive

strength of 6 ksi (41.4 MPa) used for all the specimens is provided in **Table 1**. An octagonal CFRP jacket, one layer thick, was applied for the bottom 610 mm (24 in.) of the column as shown in **Fig. 1**. The purpose of the CFRP jacket was to confine the bottom 610 mm (24 in.) of the column and postpone crushing and spalling to the column concrete.

Table 1. Concrete mix design for casting the specimens for 1 ft^3 (0.028 m^3).

Material		Specific Gravity	Weight		Volume	
			(lb.)	(kg)	(ft^3)	(m^3)
Cement		3.15	21.44	9.73	0.11	0.00305
Fly Ash		2.4	5.37	2.44	0.04	0.00100
Aggregate	Coarse Aggregate Stockton Pit #789 Aggregate	2.53	47.56	21.57	0.30	0.00843
	Fine Aggregate Valley Pit Concrete Sand	2.6	26.48	12.01	0.16	0.00457
	Fine Aggregate Stockton Pit Concrete Sand	2.596	26.44	11.99	0.16	0.00457
Water		1	10.96	4.97	0.18	0.00492
Admixture	Air Entrainer Daravair AT-30	1				
	Water Reducer Plastocrete 161	1	0.10	0.05	0.00168	0.00005
	Water Reducer High Range Visocrete 2110	1				
Air					0.05	0.00140
Total Volume:					1.00	0.028

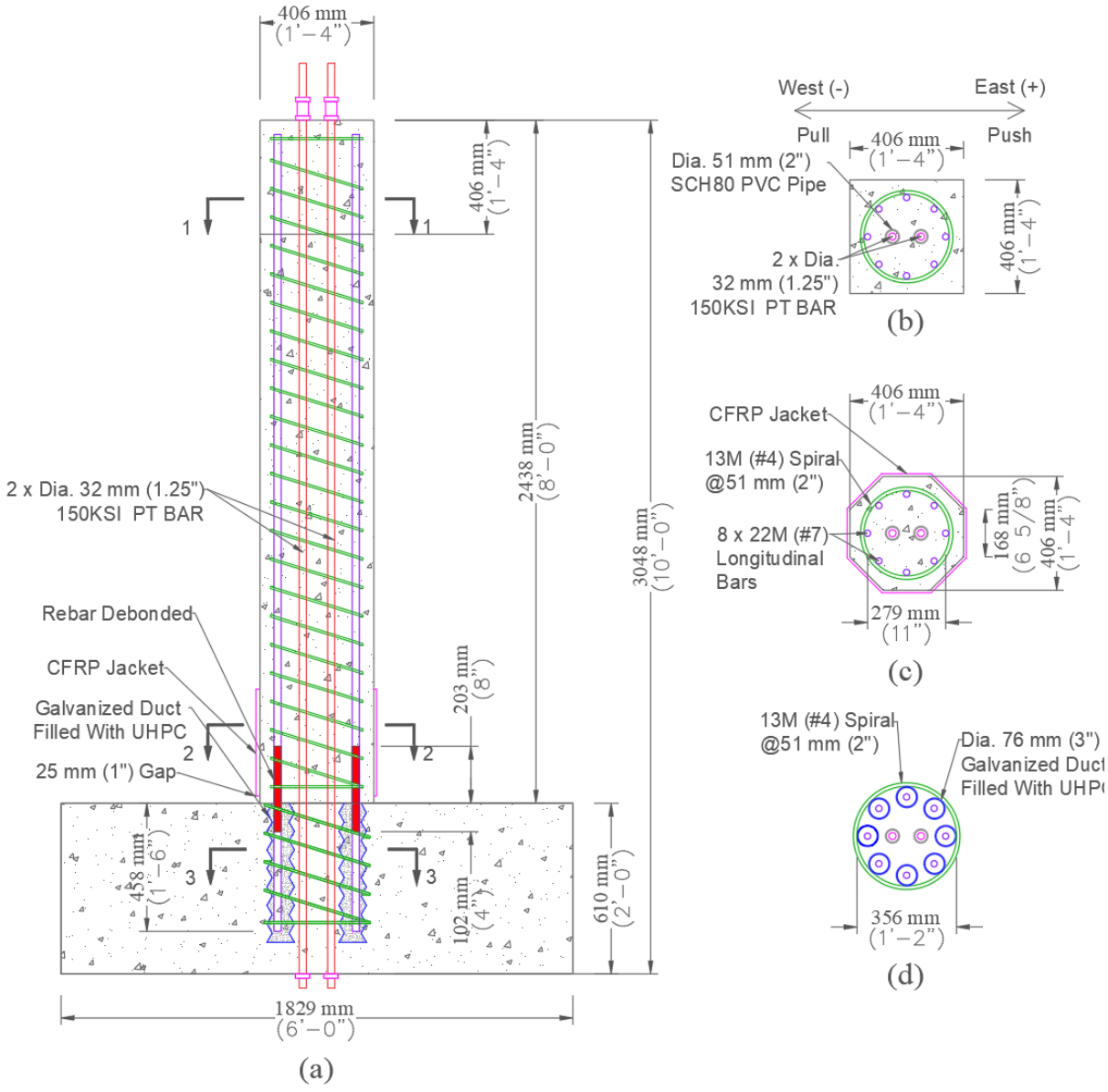

Figure 1. Specimen details: (a) column elevation; (b) section 1-1; (c) section 2-2; and (d) section 3-3.

3.1.2 FOOTING DESIGN

The column design inhibits shear failure from occurring in the column; the column failure mode is set to be either flexural or splice failure. The footing was designed to remain elastic; it was designed as a 01.83 m x 0.91 m x 0.61 m (6ft x 3ft x 2ft) precast concrete element reinforced with 25M (No. 8) longitudinal bars enclosed by 13M (No. 4) double hoops, as shown in **Fig. 2**. The footing core had eight galvanized ducts to enable joining the column to the footing. Additionally the footing and column had two PVC pipes to accommodate the PT bars after casting.

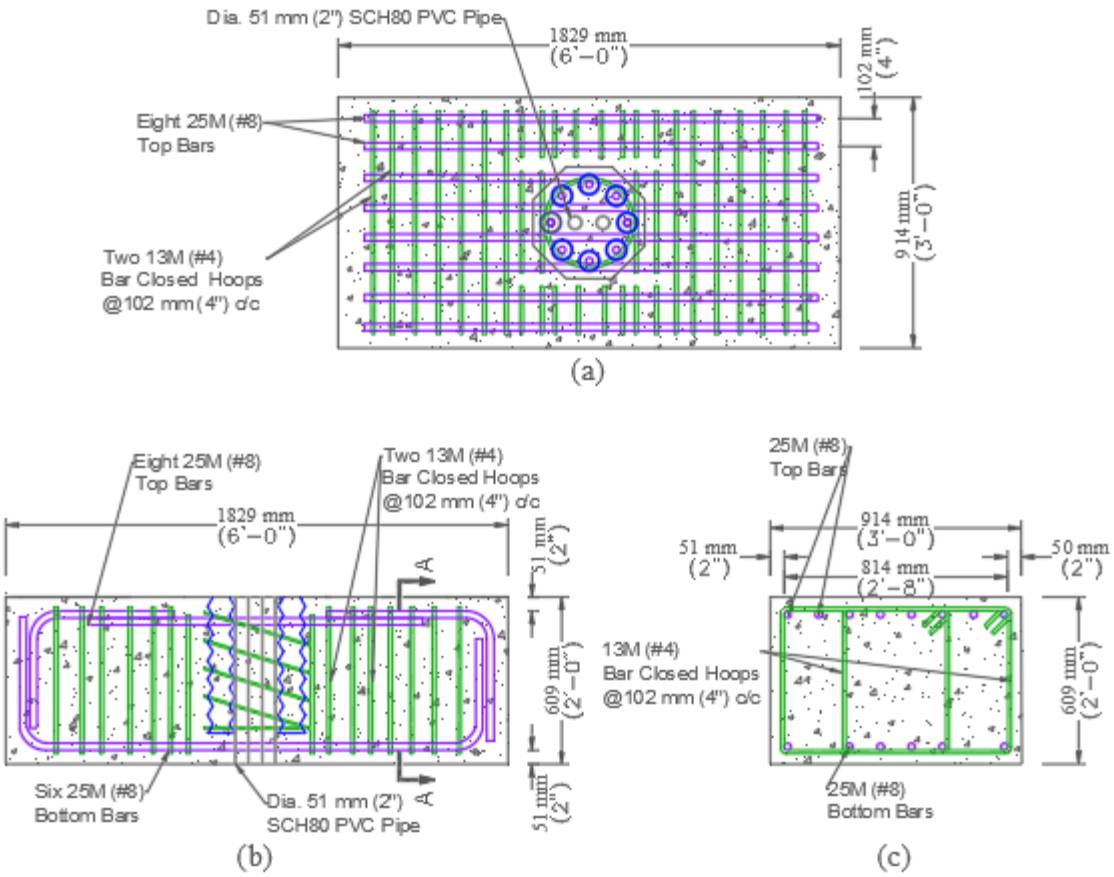

Figure 2. ABC footing details and section: (a) top view, (b) elevation, and (c) section A-A.

3.1.3 COLUMN TO FOOTING CONNECTIONS

The column is connected to the footing using the duct and grout method. The ducts need to be sturdy so as not to move during casting; thus, they are tied down to the longitudinal and transverse bars in the footing.

During the assembly procedure of the column to the footing, high-strength grout was poured into the ducts, and the column was lowered while aligning the steel reinforcing bars extending from the column. The column was supported using temporary wood bracing until the grout gained the required strength. The composition of the grout is given in **Table 2**. The average compressive strength of the grout at 28 days was 12 ksi (82.74 MPa).

Table 2. Grout mix design for 1 ft^3 (0.028 m^3).

Material	Specific Gravity	Weight		Volume	
		lbs	kg	ft^3	m^3
Sand	2.59	96.97	43.98	0.60	0.01680
Silica	2.2	5.87	2.66	0.04	0.00120
Cement	3.15	33.25	15.08	0.17	0.00474
Water	1	11.74	5.32	0.19	0.00527
Total Volume:				1.00	0.028

3.1.4 COLUMN REPAIR

The fifth specimen was constructed as an ABC column-to-footing specimen with a grouted connection, similar to the details shown in Figs. 1-3 but without post-tensioning bars (Shrestha and Pantelides 2024a; b). After it was corroded, this specimen was repaired using a CFRP shell filled with concrete; vertical-headed steel bars were epoxied into the footing to transfer tension forces to the column, as shown in **Fig. 3**. In this repair, six 22M (#7) headed steel bars were embedded 483 mm (19 in.) into the footing using high strength epoxy satisfying the development length criteria of ACI 318 (ACI 318-14). The headed steel bars' yield strength and ultimate strength were 427 MPa (62 ksi) and 593 MPa (86 ksi) respectively. Five CFRP hoop layers and two vertical CFRP layers were used to create a 610 mm (24 in.) diameter CFRP shell that was filled with concrete, as shown in Fig. 3; this design was based on previous research (Wu and Pantelides 2017). The CFRP composite's ultimate tensile strength and modulus of elasticity were 780 MPa (113 ksi) and 65 GPa (9430 ksi). The 28-day compressive strength of the concrete used inside the CFRP shell was 46.2 MPa (6.7 ksi). A 610 mm (24 in.) height was chosen for the CFRP shell since damage to the corroded specimen was concentrated in this area. A CFRP shell diameter of 610 mm (24 in.) was used to accommodate the 51 mm (2 in.) diameter head of the headed steel bars and create a clear cover to avoid contact with the column or CFRP shell. The CFRP shell was prepared separately and lowered on the column. The steel collar with steel studs was attached to the column to better bond the new concrete inside the CFRP shell to the original column concrete.

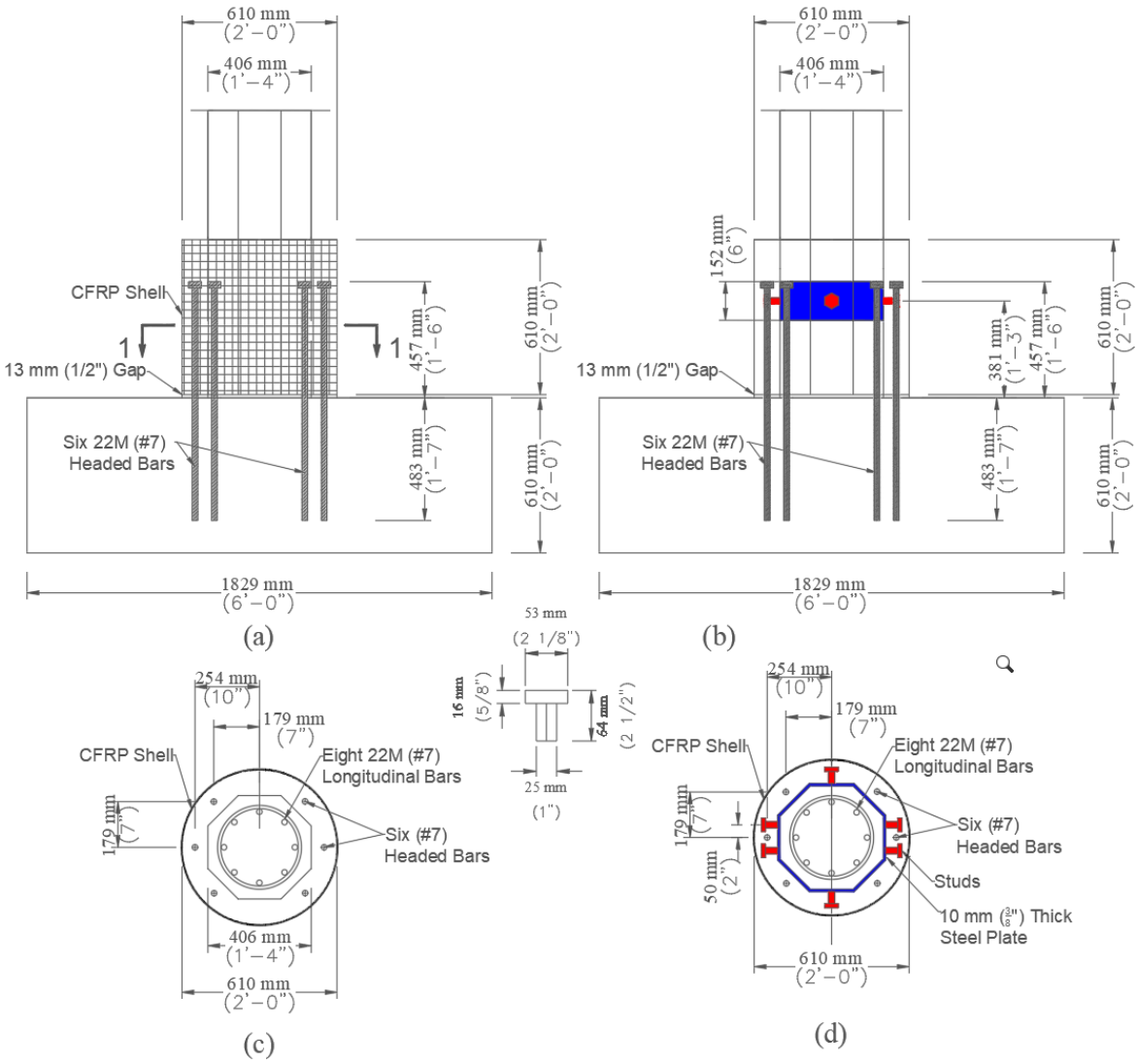

Figure 3. Column seismic repair details: (a) setup; (b) steel collar setup; (c) section 1-1; and (d) plan view.

3.1.5 POST-TENSIONING BARS

Two PT bars were placed in the columns of each of the four specimens to promote recentering of the column after earthquakes. The PT bars used in this experiment were unbonded all-threaded, 25M (No. 8) diameter bars with a minimum net area of 548 mm^2 (0.85 in.^{2}) and a tensile strength of 1034 MPa (150 ksi). The PT bars were cold-stressed and manufactured in compliance with A722/A722M-15 (ASTM 2015). The yield force of the PT bars was 454 kN (102 kip) and the ultimate force was 569 kN (128 kip).

The initial PT force in the PT bars was carefully selected to ensure that they did not yield at the end of the

test, even when subjected to a 10.0% drift ratio. Additionally, the initial PT force should not exceed 50% of the ultimate (FHWA 2013). Therefore, rigid body analogy for the column was carried out to determine the initial PT forces. The variation of PT forces for different levels of initial PT force is shown in **Fig. 4**. The initial PT force was selected to be 191 kN (43 kip) in each PT bar. The initial PT force is 0.38 times the yield force and 0.33 times the ultimate force of the PT bars used in the experiment.

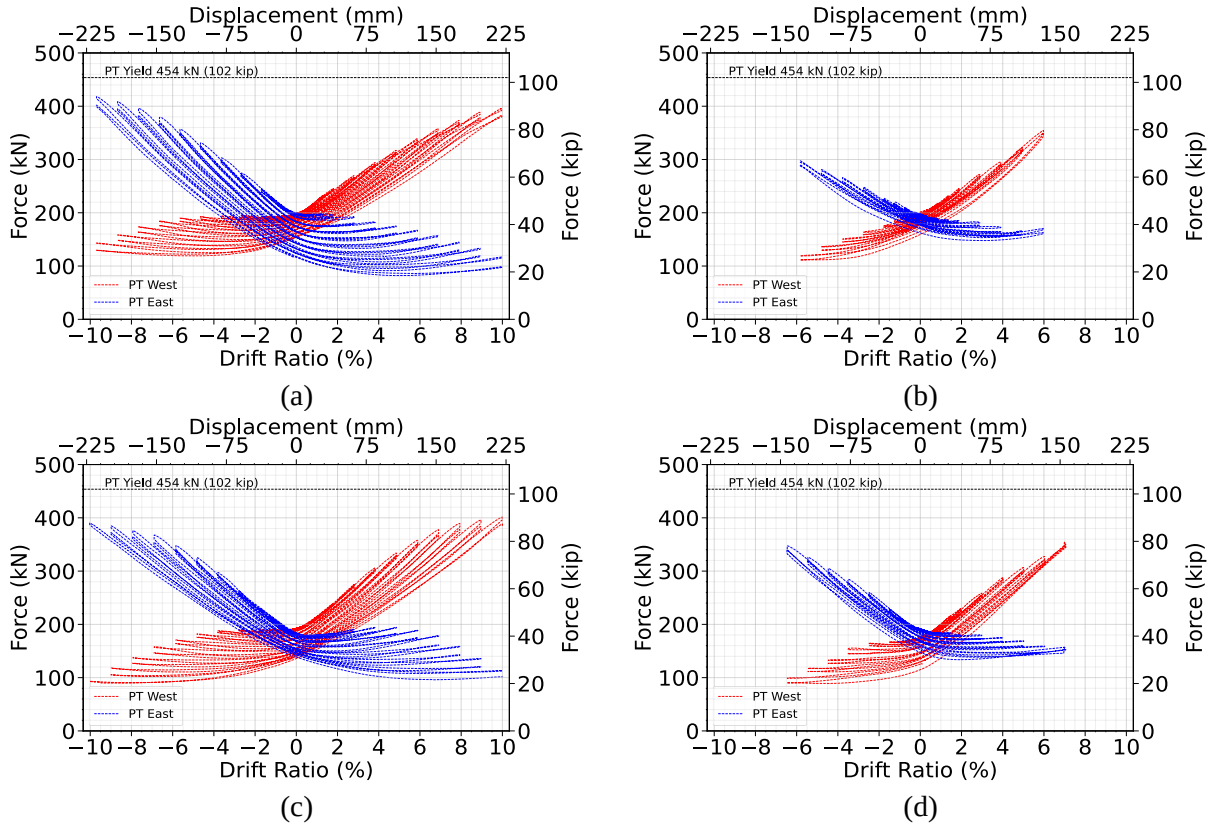

Figure 4. PT forces in the four specimens: (a) AS control; (b) AS corroded; (c) HYB control; and (d) HYB corroded.

The actual applied forces in the PT bars are shown in **Table 3**. The variation in the PT force during the test is illustrated in **Fig. 4**. It's evident that the maximum PT force falls below the yield force of the PT.

Table 3. Initial PT forces for four specimens.

Specimen	Initial PT Bar Force, kN (kip)	
	East	West
CN-AS	201(45.2)	199 (44.7)
CR-AS	200 (45.0)	201 (45.1)
CN-HYB	184 (41.3)	192 (43.2)
CR-HYB	191 (43.0)	190 (42.7)

The fifth specimen, which was corroded and repaired before being tested under cyclic loads, did not have any PT bars.

3.2 PROCESS OF ACCELERATED CORROSION

RC column specimens in previous studies were corroded using an accelerated corrosion process using a fixed current across the reinforcement and immersion into a saltwater solution. This process was used since it significantly reduces the time required to achieve steel corrosion from natural processes in the field. The amount of steel loss was estimated using Faraday's Law and is confirmed by comparing the weight of the reinforcement cage before and after corrosion (Lee et al. 2000; Li et al. 2009). This research used this process to corrode the reinforcement located in the bottom part of the column, including the plastic hinge region, as shown in **Figure 5**

According to Faraday's Law the steel loss Δw (grams), due to uniform current I (Ampere) applied over time t (s) is given by the following equation:

$$\Delta w = \frac{MIt}{zF} \quad (1)$$

where M = atomic mass of metal (56 g/mol); z = valency of metal (2); and F = Faraday's constant (96490 C/equivalent mol). The total steel loss w_t over a given period of time is given as:

$$w_t = \frac{M}{zF} \sum \Delta t \; I_{avg} \quad (2)$$

This is not the direct way of measuring corrosion as it occurs since the current is being measured and not an actual mass. The percentage mass loss is calculated by dividing the calculated mass loss with the original mass of the reinforcing bars.

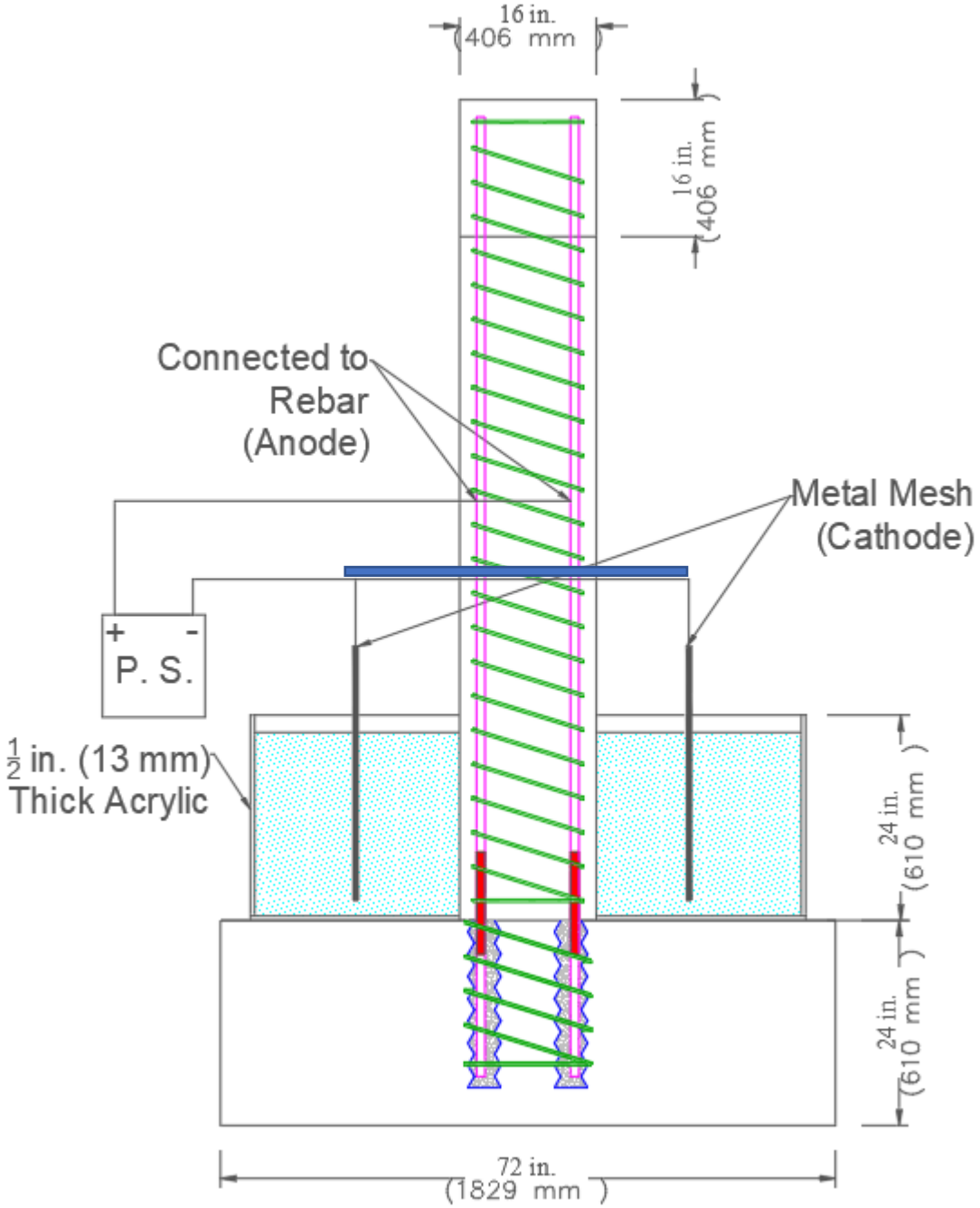

Figure 5. Accelerated corrosion setup.

The accelerated corrosion setup is shown in **Figure** 5 **5**. A 5% NaCl-water solution by weight was placed around the base of the column; to facilitate this, five plexiglass (four vertical and one horizontal) plates were used to create a water-tight seal around the column. To achieve the accelerated corrosion

process, the column longitudinal steel reinforcing bars were connected to the anode, and the salt solution was connected to the cathode of the power supply. A constant direct current was applied via a power supply for 114 days. This time duration was chosen since that was the time taken for RC columns to be severely corroded with a 25.0% target mass loss of longitudinal steel bars (Shrestha and Pantelides 2024a).

There is an increase between the actual corrosion level obtained in practice and the theoretical corrosion level calculated by Faraday's law with increase of current density. The current efficiency also decreases as the current density used in accelerated corrosion increases (Sun and Qiao 2019). Thus, the current density applied for the accelerated corrosion process in this research was chosen as 400 μA/ ($cm^2$2580 μA/$in.^2$).

The height of the plexiglass container was 610 mm (24 in.) to ensure that the plastic hinge length of the column would be inside the zone where corrosion was taking place. This is especially important since under seismic load steel bars achieve the highest strain in the plastic hinge region.

4 RESULTS

4.1 EXPERIMENTAL RESULTS FOR PT TESTS

The experiments involved subjecting the reinforced concrete columns to cyclic loading until the longitudinal steel bars fractured. The hysteresis curves in **Figure** 6 **6** demonstrate wide and stable behavior for the four post-tensioned specimens. Notable events such as CFRP delamination, toe crushing, CFRP rupture, concrete spalling, and steel bar fracture are marked. The construction materials used in the specimens were tested during the day of the experiment. The reinforcing bars had an average yield strength of 469 MPa (68ksi) and ultimate strength of 641 MPa (93ksi). Compression tests were performed using concrete and ultrahigh performance grout (UHPG) cylinders which were prepared during casting and grouting of the specimens, respectively.

AS Control Specimen

The hysteric response of the AS control specimen is shown in Fig 6(a). The control specimen was able to reach a drift of 10.0% with a maximum lateral force of 145 kN (32.5 kip). The lateral force of the column reached a plateau after achieving the maximum value without a significant drop in capacity until the end of the experiment. Vertical and horizontal cracking of the CFRP jacket could be observed at a drift ratio of 3.0%. Additionally, cracking of the concrete exposed near the toe of the column was seen at a drift ratio of 2.0%. At a drift ratio of 7.0% the CFRP layer ruptured which lead to a decrease in concrete confinement of the column. The unconfined concrete which had cracked below the CFRP layer started to spall after the CFRP jacket started to rupture near the base of the column. The spalling continued to increase till the steel spirals were exposed. The forces in the PT bars kept increasing up-to a max value of 418 kN (94.0 kip)at the 10.0% drift ratio. The experiment was stopped after the 10.0% drift cycle to prevent yielding of the PT bars used for self-centering. The condition of the specimen at the end of the test is shown in **Fig. 8(a).** The longitudinal rebar could be observed due to the spalling of the concrete near the base of the column.

AS Corroded Specimen

The hysteric response of the AS corroded specimen is shown in Fig. 6(b) . The specimen had` been damaged due to the accelerated corrosion process. Cracks could be seen in the exposed part of the column near the column-to-footing connection. Similarly, brown patches could be seen on the surface of the CFRP jacket which indicate that corrosion of the steel bars had occurred , as shown in **Fig. 7 (a)**. The corroded AS specimen reached a drift ratio of 5.0% before the first longitudinal bar fractured. A second longitudinal bar fractured at a drift ratio of 6.0%. The maximum lateral force was 107 kN (24.2 kip) during the 3.0% drift ratio cycle after which the lateral force resisting capacity of the column dropped significantly. The CFRP jacket started to delaminate at a drift ratio of 1.5% and ruptured at a drift of 2.0%. After the CFRP jacket ruptured, loss in concrete confinement of the column coupled with cracks due to corrosion caused massive spalling of concrete. The spiral reinforcement had corroded significantly thus reducing confinement of the core concrete which decreased the lateral force and displacement capacity of the column. Spalling started during the 3.0% drift ratio and continued until the end of test at which all the cover concrete had spalled exposing the corroded spiral reinforcement. The experiment was terminated after the second cycle of the 6.0% drift ratio during which the two longitudinal reinforcing bars had fractured. The maximum force in the PT bars was 373 kN (84.0 kip). The condition of the specimen at the end of the test is shown in **Fig. 8(c).**

HYB Control Specimen

The HYB control specimen had a hysteresis with wide stable loops as shown in **Fig. 6(c)** . The specimen reached a drift equal to 10.0% with a maximum lateral force of 153 kN (34.44 kip) before the experiment was terminated. The hysteresis curves show a plateau of lateral force after the peak which starts to drop after the 7.0% drift ratio cycle. The CFRP layer started to delaminate during the 3.0% drift ratio cycle and ruptured during the 6.0% drift ratio. Cracks at the toe of the column were observed at a drift ratio of 4.0% after which concrete spalling started. After the CFRP jacket ruptured at 6.0% drift ratio, the concrete above the exposed part, which was previously confined by the CFRP jacket started to spall. A drop in the lateral force occurred after the unconfined concrete had cracked and started to spall. The PT forces

reached a peak value of 401 kN (90.2 kip)at a drift ratio of 10.0%. The experiment was terminated at the 10% drift ratio cycle during which the lateral force had dropped 20% from the peak value. The condition of the specimen at the end of the test is shown in **Fig. 8(b).**

HYB Corroded Specimen

The HYB corroded specimen reached a maximum drift of 7.0% before a longitudinal reinforcing bar fractured and a maximum lateral force reached 129 kN (28.9 kip), as shown in the hysteresis curves of **Fig. 6(d).** The column had been damaged during the accelerated corrosion process. Cracks could be seen in the exposed concrete near the column-to-footing connection, as shown in **Fig. 7 (b)**. The CFRP jacket started to delaminate at 1.5% drift ratio and ruptured at the 2.0% drift ratio. However, the lateral force continued to increase; this can be attributed to the confinement provided by the GFRP spiral which was not affected by corrosion. Spalling of the cover concrete started at 3.0% drift ratio after the CFRP jacket had ruptured which continued until the GFRP spiral was exposed. The maximum force in the PT bars was 380 kN (85.5 kip). The experiment was terminated after the first cycle of the 7.0% drift ratio after the longitudinal steel bar had fractured and the lateral force had dropped. The GFRP spiral was exposed at the end of the test; the GFRP spiral was not affected by the corrosion and continued to provide confinement to the core concrete. However, the longitudinal steel bars had corroded, and the cover concrete had cracked, which resulted in a reduction of lateral force and displacement capacity of the column. The condition of the specimen at the end of the test is shown in **Fig. 8(d).**

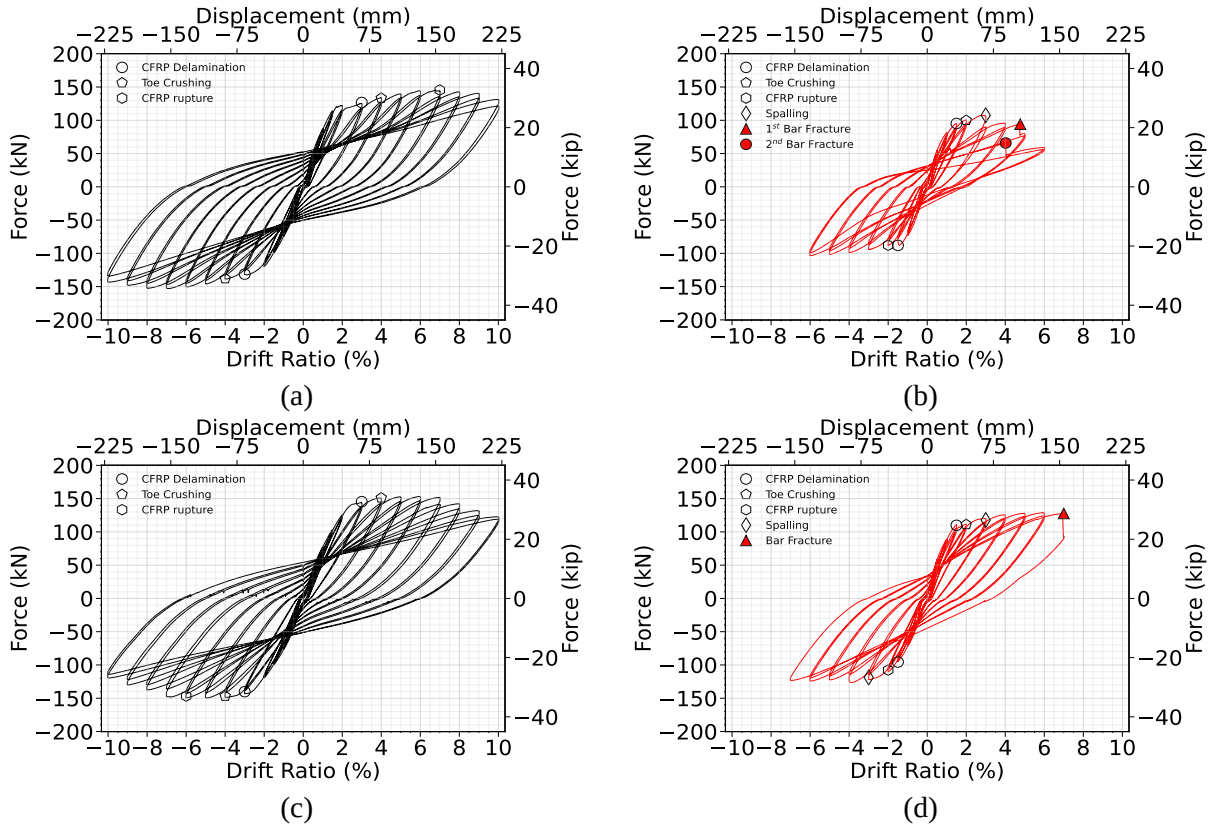

Figure 6. Hysteretic performance of specimens: (a) AS control; (b) AS corroded; (c) HYB control; and (d) HYB corroded.

(a) (b)

Figure 7. Start of test state of corroded specimens: (a) AS; and (b) HYB.

(a)

(b)

(c)

(d)

Figure 8. End of test state of specimens: (a) AS control; (b) HYB control; (c) AS corroded; and (d) HYB corroded.

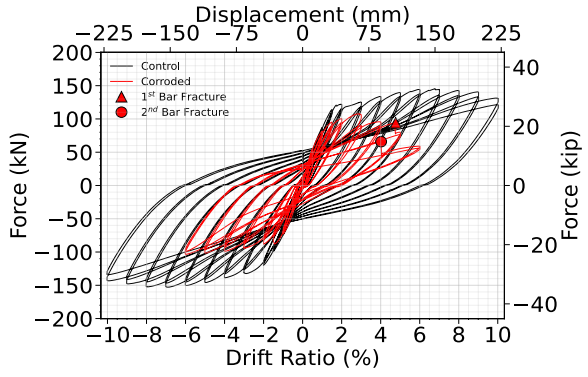

(a)

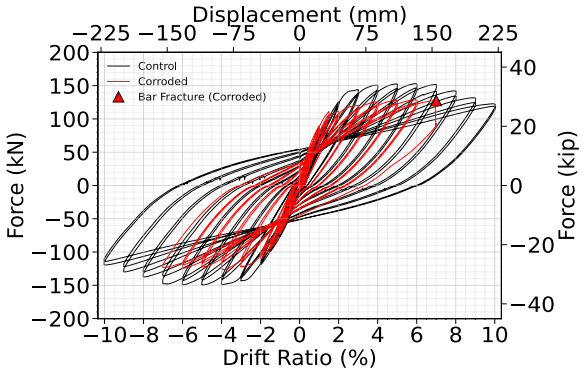

(b)

Figure 9. Comparison of hysteretic performance of control and corroded specimen for: (a) AS specimen; and (b) HYB specimen.

4.1.1 CORRODED STEEL REINFORCEMENT DETAILS

After conducting the experiments, the corroded longitudinal steel reinforcing bars were removed and weighed to determine the mass loss caused by accelerated corrosion. The rebars after being removed from the columns are shown in **Fig. 10**. The average mass loss of the longitudinal steel bars is presented as a percentage in **Table 4**. The AS corroded specimen had an average mass loss of 21.1% in the longitudinal reinforcing bars and 20.3% in the spiral reinforcement. The HYB corroded specimen had an average mass loss of 16.6% in the longitudinal reinforcing bars and the GFRP spirals were not affected by the corrosion process. The specimens were put through the accelerated corrosion process to achieve a target mass loss of 25.0% in the longitudinal reinforcement. Notably, the single layer of CFRP jacket was able to reduce the corrosion of the steel reinforcement in the AS and HYB corroded specimens. Moreover, the use of a GFRP spiral instead of a steel spiral reduced the corrosion in the longitudinal steel reinforcement of the HYB specimen to an even greater extent.

The steel spiral in the AS corroded specimen was removed and weighed after the experiments. Pitting corrosion areas were observed where the spiral and longitudinal steel reinforcement came into contact. The AS corroded specimen had localized area loss of 90% to 100% or complete area loss of the spiral steel reinforcement in certain locations.

Table 4. Average mass

ID	Specimen	Target mass loss (%)	Average Mass Loss (%)	
			Longitudinal	Spiral
RC	Severe	25	24.1	39.9
AS	All Steel	25	21.1	20.3
HYB	Hybrid	25	16.6	0.0*
*GFRP spirals present				

Figure 10. Rebar removed from corroded specimens: (a) longitudinal AS ; (b) steel spirals AS; (c) longitudinal HYB; and (d) GFRP spirals HYB.

4.1.2 DISPLACEMENT DUCTILITY AND STIFFNESS

The displacement ductility capacity was determined by constructing backbone curves using peak force values at each drift ratio, as shown in **Fig. 11**. The effective yield and ultimate displacement were calculated based on an equal energy of the idealized elastoplastic system. The ultimate displacement was determined at a drift ratio where either bar fracture or a 20% drop in lateral force capacity occurred, whichever came first. The displacement ductility, defined as the ratio of ultimate to yield displacement, decreased with corrosion. The AS specimen had a displacement ductility of 5.1 and 4.7 for the control and corroded specimens, respectively. The HYB specimen had a displacement ductility of 4.7 and 4.4 for the control and corroded specimens, respectively.

The stiffness of the corroded specimens in the push and pull cycles varied due to different levels of corrosion in the longitudinal steel bars on the east and west sides of the column, as shown in Figure 11. The initial stiffness of all the specimens was similar. However, the peak lateral force of the corroded specimens was significantly lower than the control specimens. The control specimens exhibited a lateral force plateau after reaching the peak force, whereas the corroded specimens experienced a noticeable decrease in lateral force, which was particularly evident in the case of the AS corroded specimen.

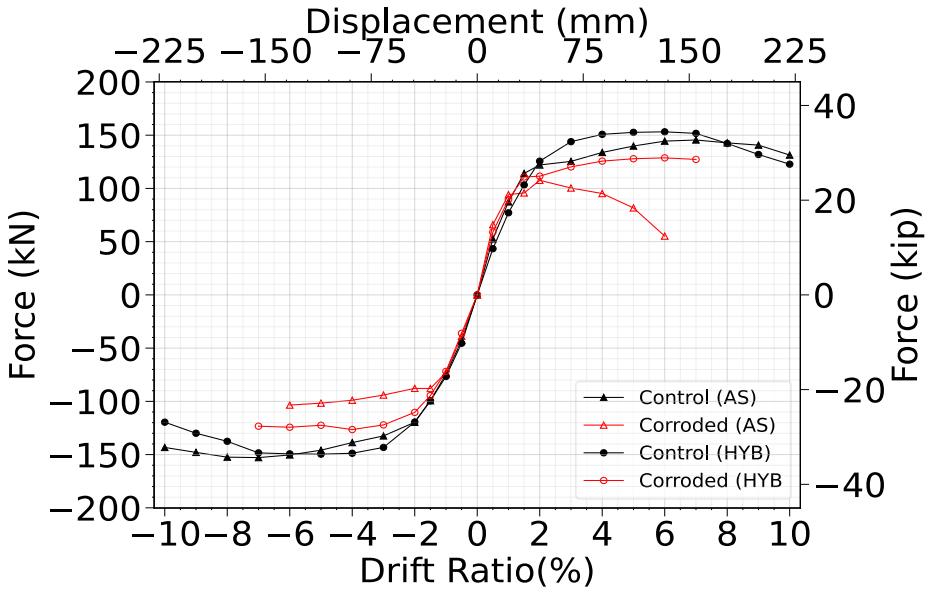

Figure 11. Force displacement response backbone for the four post-tensioned specimens.

4.1.3 SELF CENTERING CAPACITY AND RESIDUAL DRIFT

The four post-tensioned specimens in this study were constructed with PT bars to increase the self-centering capacity of the columns. **Figure 12** shows the residual drift of the four columns. The residual drift of the corroded columns is compared to the control columns in the case of both the AS and HYB specimens. The HYB specimen at a certain drift ratio has a better self-centering behavior than the AS specimen. Even the corroded HYB specimen had better self-centering than the control AS column. This is due to the GFRP spirals not deteriorating during the accelerated corrosion of the specimens. The corroded HYB specimen still had similar core concrete confinement to the control HYB specimen. However, the AS specimen lost concrete core confinement due to corrosion of the steel spiral which caused further decrease in self-centering of the column.

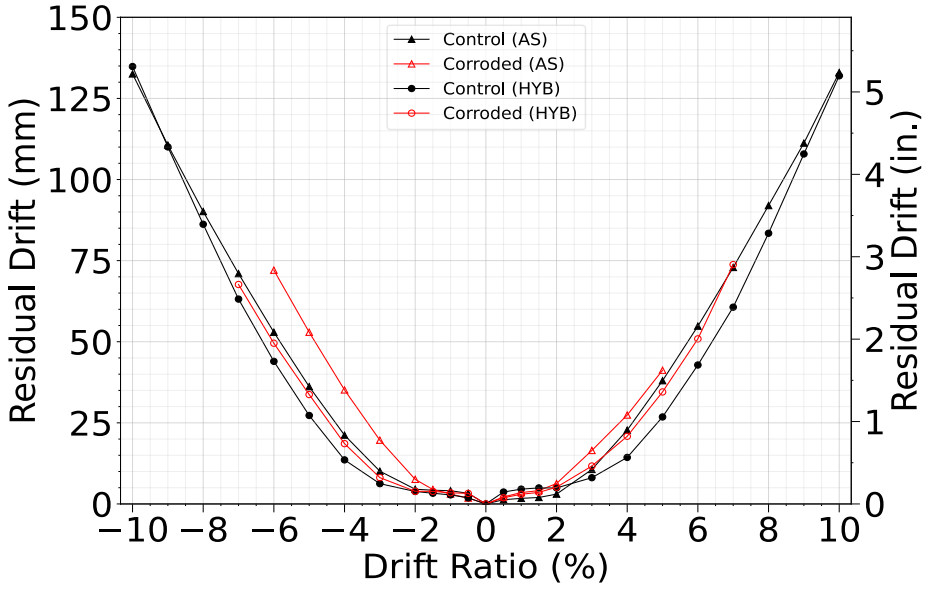

Figure 12. Residual drift.

4.1.4 HYSTERETIC ENERGY DISSIPATION AND COLUMN CURVATURE PROFILES

Figure 13(a) shows the cumulative hysteretic energy capacity. Up to a 5.0% drift ratio, the four post-tensioned specimens exhibit similar energy dissipation; however, the two corroded specimens show reduced hysteretic energy dissipation beyond that point. The cumulative hysteretic energy dissipated by the corroded specimens is 78.0% and 60.0% less than the control specimen for the AS and HYB specimens,

respectively before the longitudinal bar fractures.

Figure 13(b) displays values of equivalent viscous damping ratio. Corroded columns show increased hysteretic damping due to a sharp decrease in strain energy compared to the decrease in the hysteretic energy.

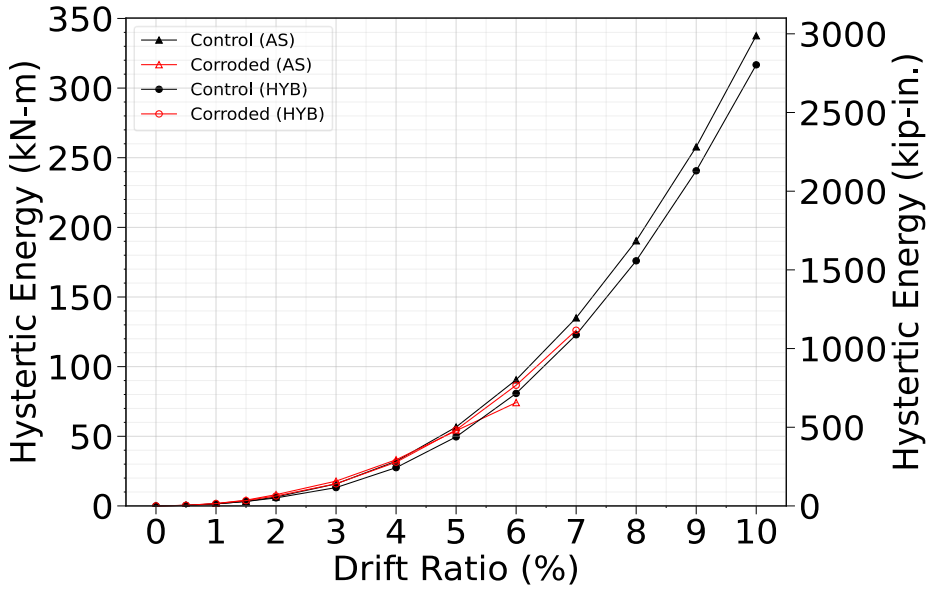

(a)

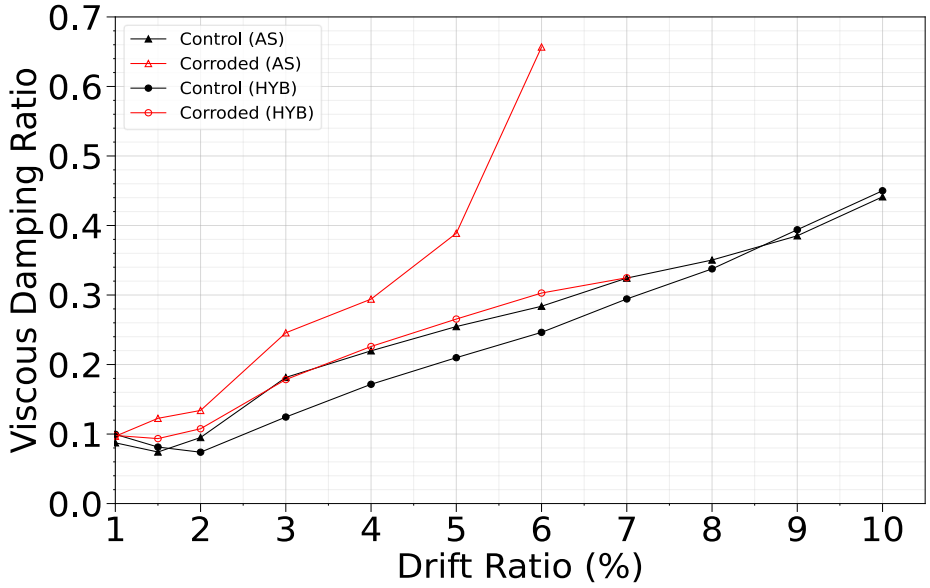

(b)

Figure 13. Energy dissipation capacity: (a) cumulative hysteretic energy; and (b) equivalent viscous damping ratio.

Normalized curvature is defined as curvature times the column width. Normalized curvature

profiles are shown in **Fig. 14.** for the four post-tensioned columns. These profiles show increased curvature in the corroded region of the column, especially in the 203-406 mm (8-16 in.) range above the footing.

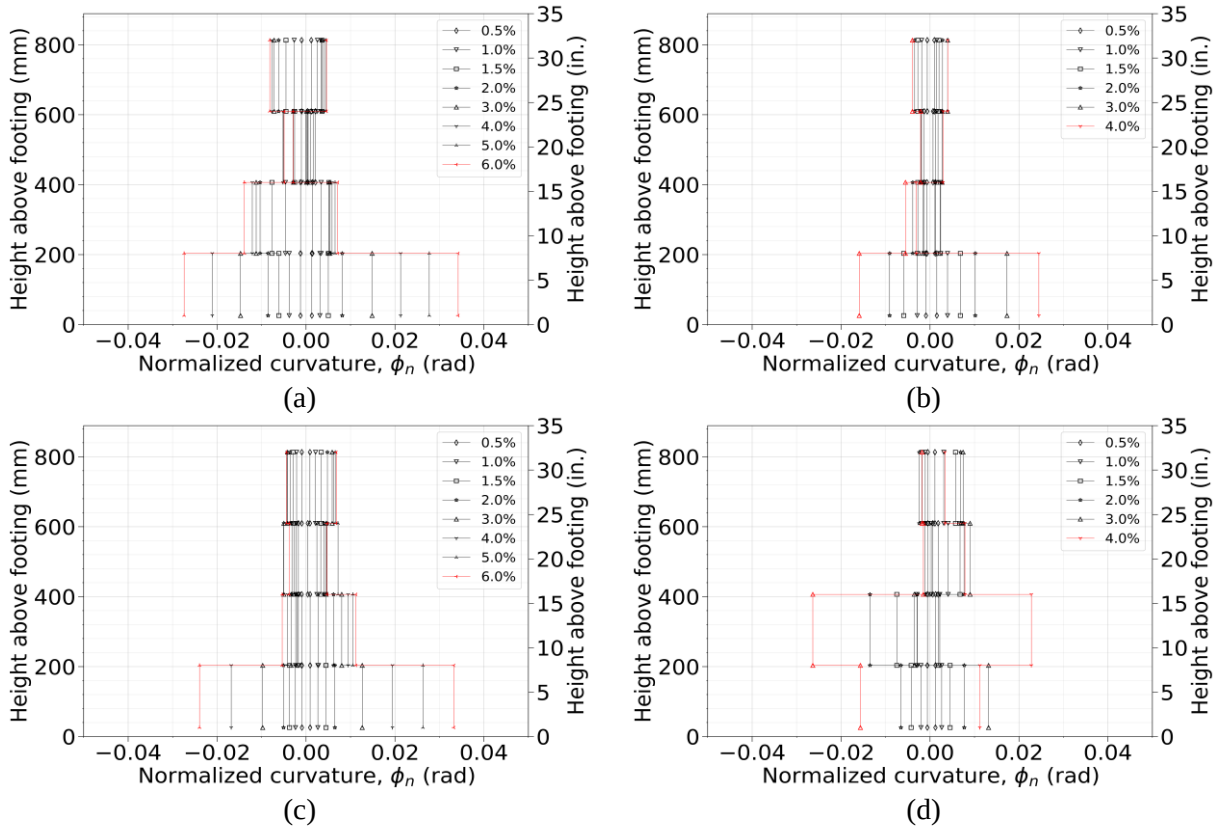

Figure 14. Normalized curvature of specimens: (a) AS control; (b) AS corroded; (c) HYB control; and (d) HYB corroded.

The strain in the east and west longitudinal bar of the control specimen of the AS and HYB specimen is shown in **Fig. 15**. Strain gauges attached to the longitudinal steel bars show yielding along the instrumented height up to 406 mm (16 in.). Additionally, the strain in the steel spiral for the AS specimen and the GFRP spiral in the HYB specimen in shown in **Fig. 16**. Strain gauges in the corroded specimens were damaged during accelerated corrosion.

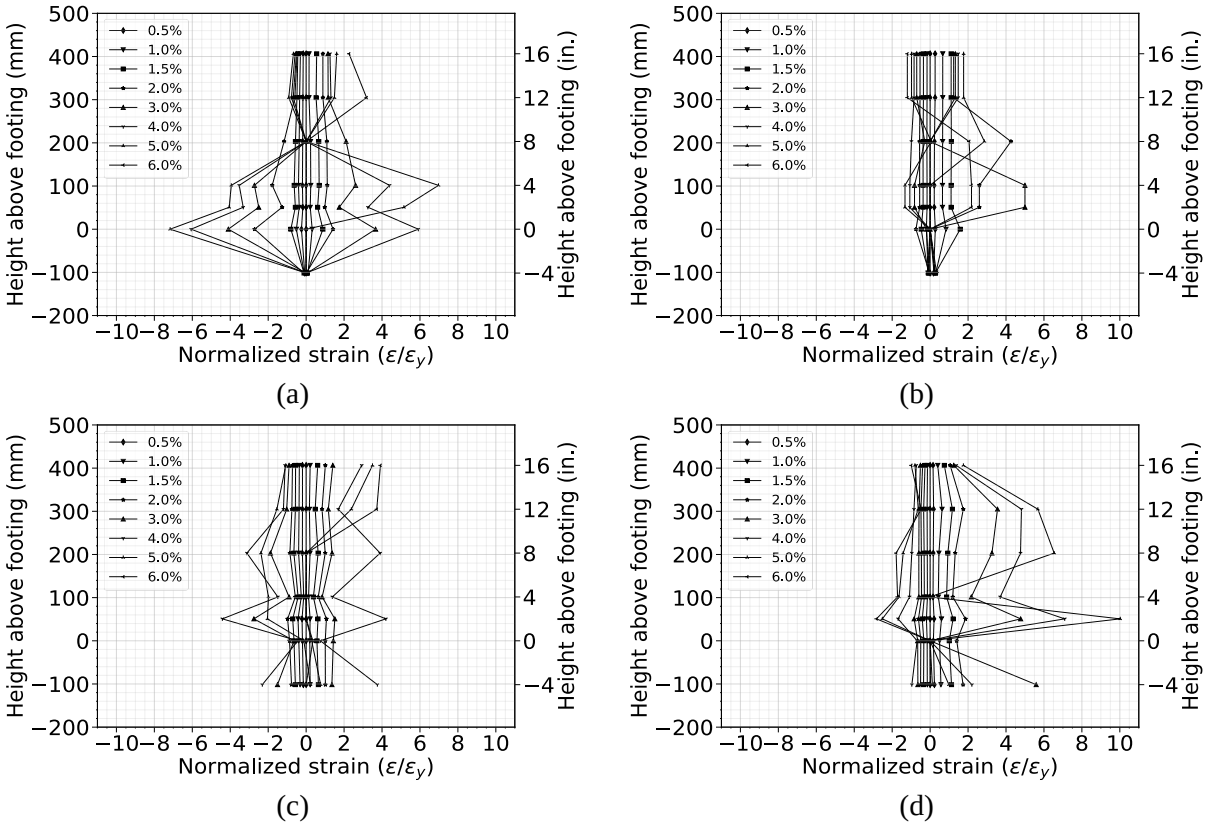

Figure 15. Strain in longitudinal bar for control specimen: (a) AS east; (b) AS west; (c) HYB east; and (d) HYB west.

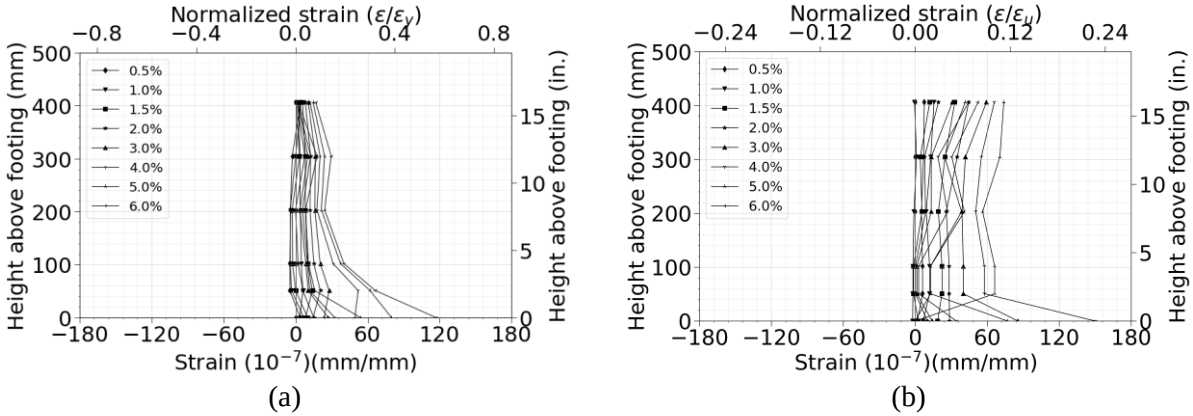

Figure 16. Strain in spiral reinforcement control specimen: (a) AS steel spiral; and (b) HYB GFRP spiral.

4.2 EXPERIMENTAL RESULTS FOR REPAIRED COLUMN

The hysteresis response of the repaired specimen is shown in **Fig. 17**. A maximum lateral force of 180 kN (40.5 kip) was achieved at a drift ratio of 4.0%. After the peak value was reached, the lateral force dropped in subsequent cycles until bar fracture at 10.0% drift ratio. The repaired specimen developed hairline cracks above the CFRP shell during the 2.0% drift ratio cycle. At 3.0% drift ratio, spalling occurred with cracks extending from the CFRP shell up to a height of 813 mm (32 in.). At the 4.0% drift ratio, the cracks reached a width of 1 mm (0.04 in.) and concrete spalling was initiated. The steel spirals became visible once all cover concrete was lost due to spalling at the 6.0% drift ratio. A discernible decline in lateral force, amounting to 10% reduction of the maximum lateral force was observed at 7.0% drift ratio, which intensified during the 9.0% drift ratio. A longitudinal steel bar ruptured during the second cycle of the 10.0% drift ratio when the test was terminated. The cumulative hysteretic energy dissipation and equivalent viscous damping ratio for the control (Shrestha and Pantelides 2024) and repaired specimen after corrosion are shown in **Fig. 18(a)** and **Fig. 18(b),** respectively. The repaired specimen dissipated a cumulative hysteretic energy of 491 kN-m (4344 kip-in.) before fracture of a longitudinal steel bar at 10.0% drift ratio.

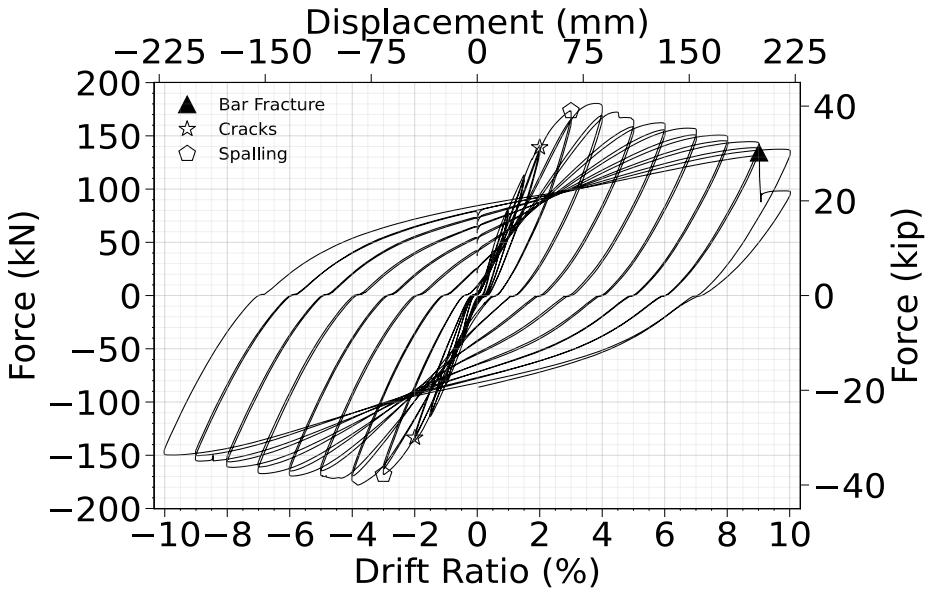

Figure 17. Hysteresis of repaired specimen.

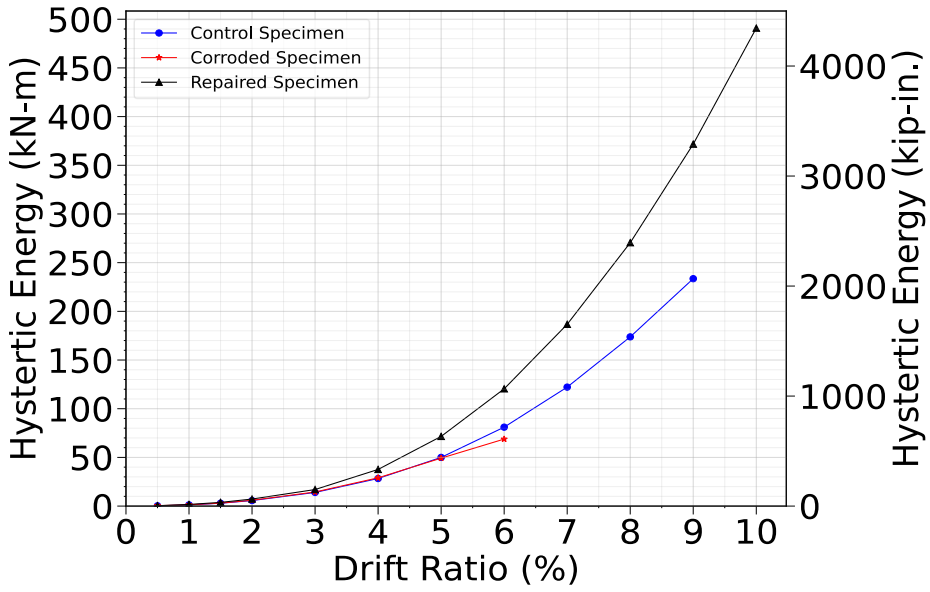

(a)

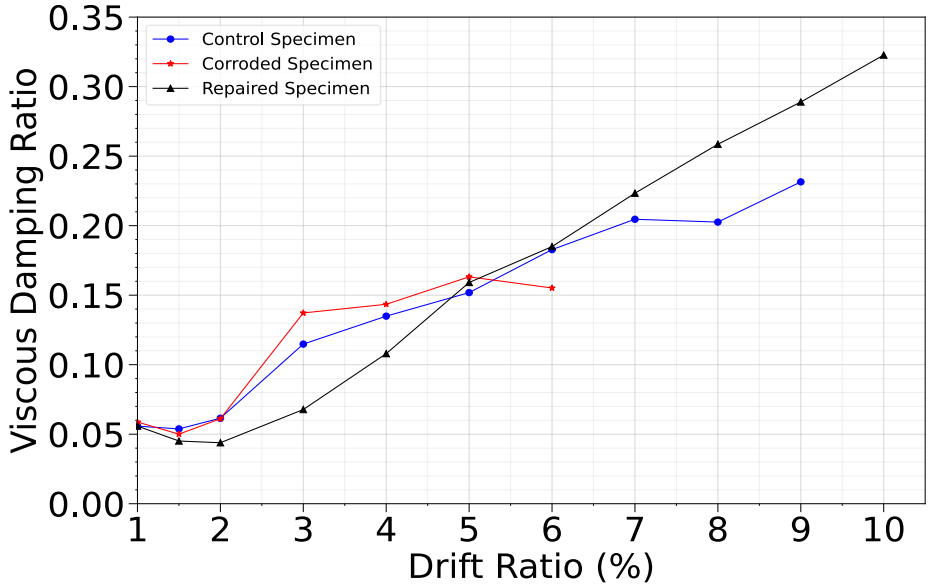

(b)

Figure 18. Comparison of repaired specimen with control and corroded specimens: (a) cumulative hysteretic energy; and (b) equivalent viscous damping ratio.

5 SUMMARY AND CONCLUSIONS

5.1 SUMMARY

The seismic performance of bridge columns built using ABC methods with PT bars subjected to accelerated corrosion was studied. For this study four columns were constructed: two with steel spirals (AS), and two with GFRP spirals (HYB). The two types of spiral material were examined to determine the level of protection offered by the GFRP spiral to the longitudinal steel bars compared to the steel spiral. The research in this study studies the difference in seismic performance of the control (CN) and corroded (CR) specimens with the steel and GFRP spiral. Additionally, the difference in the mass loss due to corrosion in the longitudinal steel bars while using steel and GFRP spiral is studied.

The repair of a corroded column repaired using CFRP shell and headed steel bars was also studied. The results are compared to a control specimen and corroded specimen of similar construction but without post-tensioning bars.

5.2 CONCLUSIONS

This research examined the cyclic capacity of columns constructed using accelerated bridge construction methods with debonded longitudinal steel reinforcing bars and post-tensioning bars, after being exposed to severe corrosion. There are two types of columns in this study; two constructed using steel spirals and two constructed using GFRP spirals. The research findings are as follows:

(i) The control specimens of both the AS and HYB columns did not experience longitudinal steel bar fracture until the end of the test at the 10.0% drift ratio cycle. The corroded specimens experienced longitudinal bar fracture during the 5.0% and 7.0% drift ratio for the AS and HYB specimens, respectively; this was because corrosion of longitudinal steel and cracking of cover concrete due to corrosion.

(ii) Lateral force capacity and cumulative hysteretic energy decreased with corrosion. Compared to the control specimen, the corroded specimens had lower peak lateral forces by 26.0% and

16.0%, respectively for the AS specimen and HYB specimen. Cumulative hysteretic energy was lower by 78.0% and 60.0%, for the AS and HYB specimens, respectively.

(iii) The accelerated corrosion tests on AS and HYB columns showed significant differences in mass loss of longitudinal steel bars: 21% for AS and 16.6% for HYB, with spiral steel reinforcement in AS experiencing a 20.3% loss. Despite equal exposure durations, the GFRP spiral effectively inhibited corrosion in the longitudinal bars. Adding a single layer of CFRP jacket reduced corrosion in AS to 21%, and GFRP spirals in HYB further mitigated losses to 16.6%. These findings underscore the protective efficacy of GFRP and CFRP in enhancing the durability of reinforced concrete structures under corrosive conditions.

(iv) The corroded specimens exhibited cracks in the exposed concrete within the column-to-footing connection zone. In both the AS and HYB control specimens, the CFRP jacket began to delaminate from the concrete, with circumferential and vertical cracks observed at a 2.0% drift ratio. Similarly, in the corroded specimens, delamination of the CFRP jacket from the concrete was evident even before cyclic testing began. The CFRP jackets in the corroded specimens started to crack from the beginning of the test.

(v) In the control specimens, CFRP rupture occurred at a 7.0% and 6.0% drift ratio in the AS and HYB columns, respectively. For the corroded specimens, the CFRP jackets, which had already started to crack early in the test, ruptured during the 2.0% drift ratio cycle.

(vi) Corrosion of the steel spiral caused the confinement loss in the corroded AS specimen, but the GFRP spiral did not corrode so the corroded HYB specimen did not experience such loss in confinement of core concrete. Displacement ductility was reduced with corrosion, measuring 5.1 and 4.7 for the control and corroded AS specimens, respectively; displacement ductility reached 4.7 and 4.4 for the control and corroded HYB specimens, respectively.

(vii) Strain readings of the control specimens were measured for the longitudinal steel bars. The strain was observed to reach 8-10 times the yield strain of the rebar in the debonded region which showed the effectiveness of debonding to develop the desired strain in the columns. The

uniform distribution of strain in the GFRP spirals show better confinement of core concrete compared to the steel spiral.

(viii) The repair of the severely corroded column using the CFRP shell and headed steel bars restored its lateral displacement and drift capacity. The repaired specimen reached a drift ratio of 10.0%; the drift ratio achieved by the control and corroded column was 9.0% and 6.0%, respectively.

(ix) The repaired specimen could resist a higher lateral force than the control and corroded columns. The repaired specimen had a peak lateral force of 180 kN (40.5 kips); the peak lateral force achieved by the control and corroded column was 117 kN (26.3 kips) and 109 kN (24.5 kips), respectively.

(x) Corrosion of columns constructed using ABC methods has an adverse effect on displacement and lateral force capacity if the mass loss of steel bars is above 10.0%. The inclusion of GFRP spirals in new ABC constructed bridge columns improves the displacement capacity by 1.0% to 2.0% drift ratio. Repair of corroded ABC columns with a CFRP shell and headed steel bars can restore the displacement capacity of such columns.

6 REFERENCES

ACI. 2017. “ACI Committee 440: Guide for the design and construction of externally bonded FRP systems for strengthening concrete structures.” *American Concrete Institute*. American Concrete Institute.

Ahmad, S. 2003. “Reinforcement corrosion in concrete structures, its monitoring and service life prediction - A review.” *Cem Concr Compos*. Elsevier Ltd.

Akhoondan, M., and G. E. C. Bell. 2016. “Fastener Corrosion.” *Structure*, 13 (3): 74–75.

Ali, M. A., and E. El-Salakawy. 2016. “Seismic Performance of GFRP-Reinforced Concrete Rectangular Columns.” *Journal of Composites for Construction*, 20 (3). American Society of Civil Engineers (ASCE). https://doi.org/10.1061/(asce)cc.1943-5614.0000637.

Alonso, C., C. Andrade, J. Rodriguez, and J. M. Diez. 1998. “Factors controlling cracking of concrete affected by reinforcement corrosion.” *Materials and Structures/Materiaux et Constructions*, 31 (211): 435–441. RILEM Publications. https://doi.org/10.1007/BF02480466/METRICS.

Ameli, M. J., J. E. Parks, D. N. Brown, and C. P. Pantelides. 2015. “Seismic evaluation of grouted splice sleeve connections for reinforced precast concrete column-to-cap beam joints in accelerated bridge construction.” *PCI Journal*, 60 (2): 80–103. Precast/Prestressed Concrete Institute. https://doi.org/10.15554/PCIJ.03012015.80.103.

Andisheh, K., A. Scott, A. Palermo, and D. Clucas. 2019. “Influence of chloride corrosion on the effective mechanical properties of steel reinforcement.” *Structure and Infrastructure Engineering*, 15 (8): 1036–1048. Taylor and Francis Ltd. https://doi.org/10.1080/15732479.2019.1594313.

Apostolopoulos, C., A. Drakakaki, and M. Basdeki. 2019. “Seismic assessment of RC column under seismic loads.” *International Journal of Structural Integrity*, 10 (1): 41–54. Emerald Group Holdings Ltd. https://doi.org/10.1108/IJSI-02-2018-0013/FULL/XML.

Bae, S.-W., and A. Belarbi. 2009. “Effects of Corrosion of Steel Reinforcement on RC Columns Wrapped with FRP Sheets.” *Journal of Performance of Constructed Facilities*, 23 (1): 20–31.

https://doi.org/10.1061/ASCE0887-3828200923:120.

Basdeki, M., K. Koulouris, and C. Apostolopoulos. 2022. “Effect of Corrosion on the Hysteretic Behavior of Steel Reinforcing Bars and Corroded RC Columns.” *Applied Sciences 2022, Vol. 12, Page 7451*, 12 (15): 7451. Multidisciplinary Digital Publishing Institute. https://doi.org/10.3390/APP12157451.

Billington, S. L., and J. K. Yoon. 2004. “Cyclic Response of Unbonded Posttensioned Precast Columns with Ductile Fiber-Reinforced Concrete.” *Journal of Bridge Engineering*, 9 (4): 353–363. American Society of Civil Engineers. https://doi.org/10.1061/(ASCE)1084-0702(2004)9:4(353).

Campione, G., F. Cannella, and G. Minafò. 2016. “A simple model for the calculation of the axial load-carrying capacity of corroded RC columns.” *Materials and Structures/Materiaux et Constructions*, 49 (5): 1935–1945. Kluwer Academic Publishers. https://doi.org/10.1617/s11527-015-0624-4.

Choine M. N. 2014. “Seismic reliability assessment of ageing integral bridges.” Dublin, Ireland: Trinity College.

Culmo, M. P. 2011. *Accelerated Bridge Construction: Experience in Design, Fabrication and Erection of Prefabricated Bridge Elements and Systems: Final Manual*.

Dangol, I., and C. P. Pantelides. 2022. “Resilient Posttensioned Bridge Bent with Buckling Restrained Brace.” *Journal of Bridge Engineering*, 27 (2). American Society of Civil Engineers (ASCE). https://doi.org/10.1061/(asce)be.1943-5592.0001823.

Fang, C., K. Lundgren, L. Chen, and C. Zhu. 2004. “Corrosion influence on bond in reinforced concrete.” *Cem Concr Res*, 34 (11): 2159–2167. https://doi.org/10.1016/j.cemconres.2004.04.006.

Fang, C., Z. Yuan, S. Yang, and J. Zhang. 2017. “Performance of corroded bridge piers under cyclic loading.” *Proceedings of the Institution of Civil Engineers: Bridge Engineering*, 170 (4): 255–270. Thomas Telford Services Ltd. https://doi.org/10.1680/jbren.16.00001.

FHWA. 2013. “Post-Tensioning Tendon Installation and Grouting Manual.” *FHWA-NHI-13-026, Version 2, Washington, DC: FHWA.*

Gergely, J., C. P. Pantelides, and L. D. Reaveley. 2000. “Shear strengthening of RCT-joints using CFRP composites.” *Journal of Composites for Construction*, 4 (2): 56–64.

https://doi.org/10.1061/(ASCE)1090-0268(2000)4:2(56).

Goodyear D., and Lund H. 2019. “Seismic Design of Non-Conventional Bridges.” *Seismic Design of Non-Conventional Bridges*. Transportation Research Board. https://doi.org/10.17226/25489.

Jia, J., L. Zhao, S. Wu, X. Wang, Y. Bai, and Y. Wei. 2020. “Experimental investigation on the seismic performance of low-level corroded and retrofitted reinforced concrete bridge columns with CFRP fabric.” *Eng Struct*, 209. Elsevier Ltd. https://doi.org/10.1016/j.engstruct.2020.110225.

Kazuhiko, K. 1997. “The 1996 Japanese seismic design specifications of highway bridges and the performance based design.” *Seismic Design Methodologies for the Next Generation of Codes*, 371–382. Routledge. https://doi.org/10.1201/9780203740019-33.

Kharal, Z., J. K. Carrette, and S. A. Sheikh. 2021. “Large Concrete Columns Internally Reinforced with GFRP Spirals Subjected to Seismic Loads.” *Journal of Composites for Construction*, 25 (3). American Society of Civil Engineers (ASCE). https://doi.org/10.1061/(asce)cc.1943-5614.0001121.

Kharal, Z., and S. A. Sheikh. 2020. “Seismic Behavior of Square and Circular Concrete Columns with GFRP Reinforcement.” *Journal of Composites for Construction*, 24 (1): 04019059. American Society of Civil Engineers (ASCE). https://doi.org/10.1061/(ASCE)CC.1943-5614.0000988/ASSET/2E16E4CB-471B-4D4E-8500-EA02B469A96E/ASSETS/IMAGES/LARGE/FIGURE11.JPG.

Lee, C., J. Bonacci, M. Thomas, M. Maalej, S. Khajehpour, N. Hearn, S. Pantazopoulou, and S. Sheikh. 2000. *Accelerated corrosion and repair of reinforced concrete columns using carbon fibre reinforced polymer sheets*.

Li, J., J. Gong, and L. Wang. 2009. “Seismic behavior of corrosion-damaged reinforced concrete columns strengthened using combined carbon fiber-reinforced polymer and steel jacket.” *Constr Build Mater*, 23 (7): 2653–2663. https://doi.org/10.1016/j.conbuildmat.2009.01.003.

Lin, H., Y. Zhao, J. Q. Yang, P. Feng, J. Ozbolt, and H. Ye. 2019. “Effects of the corrosion of main bar and stirrups on the bond behavior of reinforcing steel bar.” *Constr Build Mater*, 225: 13–28. Elsevier Ltd. https://doi.org/10.1016/j.conbuildmat.2019.07.156.

Mackie, K., and B. Stojadinovic. 2004. “Residual displacement and post earthquake capacity of highway bridges.” *13th World Conference on Earthquake Engineering*.

Marsh, M. L., and S. J. Stringer. 2013. *Performance-based seismic bridge design*. Washington, DC: NCHRP Synthesis-440, TRB.

Neupane, S., and C. P. Pantelides. 2024. “Hybrid bridge bent using stretch length anchors with post-tensioning and shear key alternatives.” *Eng Struct*, 310. Elsevier Ltd. https://doi.org/10.1016/j.engstruct.2024.118144.

Ou, Y.-C., P.-H. Wang, M.-S. Tsai, K.-C. Chang, and G. C. Lee. 2010. “Large-Scale Experimental Study of Precast Segmental Unbonded Posttensioned Concrete Bridge Columns for Seismic Regions.” *Journal of Structural Engineering*, 136 (3): 255–264. https://doi.org/10.1061/ASCEST.1943-541X.0000110.

Palermo, A., S. Pampanin, and D. Marriott. 2007. “Design, Modeling, and Experimental Response of Seismic Resistant Bridge Piers with Posttensioned Dissipating Connections.” *Journal of Structural Engineering*, 133 (11): 1648–1661. American Society of Civil Engineers (ASCE). https://doi.org/10.1061/(ASCE)0733-9445(2007)133:11(1648)/ASSET/7DB0BCB6-FFD0-458C-8F18-4810809A9640/ASSETS/IMAGES/LARGE/16.JPG.

Pantelides, C. P., J. Gergely, L. D. Reaveley, and V. A. Volnyy. 1999. “Retrofit of RC bridge pier with CFRP advanced composites.” *Journal of Structural Engineering*, 125 (10): 1094–1099. https://doi.org/10.1061/(ASCE)0733-9445(1999)125:10(1094).

Pantelides, C. P., M. E. Gibbons, and L. D. Reaveley. 2013. “Axial Load Behavior of Concrete Columns Confined with GFRP Spirals.” *Journal of Composites for Construction*, 17 (3): 305–313. American Society of Civil Engineers. https://doi.org/10.1061/(ASCE)CC.1943-5614.0000357.

Parks, J. E., D. N. Brown, M. J. Ameli, and C. P. Pantelides. 2016. “Seismic repair of severely damaged precast reinforced concrete bridge columns connected with grouted splice sleeves.” *ACI Struct J*, 113 (3): 615–626. American Concrete Institute. https://doi.org/10.14359/51688756.

Rajput, A. S., and U. K. Sharma. 2018. “Corroded reinforced concrete columns under simulated seismic

loading." *Eng Struct*, 171: 453–463. Elsevier Ltd. https://doi.org/10.1016/j.engstruct.2018.05.097.

Rodriguez, J., L. M. Ortega, and J. Casal. 1997. "Load carrying capacity of concrete structures with corroded reinforcement." *Constr Build Mater*, 11 (4): 239–248. Elsevier. https://doi.org/10.1016/S0950-0618(97)00043-3.

Saenz, N., and C. P. Pantelides. 2006. "Short and Medium Term Durability Evaluation of FRP-Confined Circular Concrete." *Journal of Composites for Construction*, 10 (3): 244–253. American Society of Civil Engineers (ASCE). https://doi.org/10.1061/(ASCE)1090-0268(2006)10:3(244)/ASSET/B86597F4-1BD8-4A99-B70B-F2DB38412D50/ASSETS/IMAGES/5.JPG.

Shrestha, S., and C. P. Pantelides. 2024a. "Seismic Performance of Corroded Precast Reinforced Concrete Columns with Intentional Debonding." *ACI Struct J*, 121 (4). American Concrete Institute. https://doi.org/10.14359/51740713.

Shrestha, S., and C. P. Pantelides. 2024b. "Cyclic Tests and Analysis of Corroded Precast Concrete Column-to-Footing Connections Constructed with Accelerated Bridge Construction Methods." *Journal of Bridge Engineering*, 29 (6). https://doi.org/10.1061/JBENF2.BEENG-6632.

Sideris, P., A. J. Amjad, and A. Filiatrault. 2014. "Large-Scale Seismic Testing of a Hybrid Sliding-Rocking Posttensioned Segmental Bridge System." *Journal of Structural Engineering*, 140 (6): 04014025–1. https://doi.org/10.1061/(ASCE)ST.

Soudki, K., E. El-Salakawy, and B. Craig. 2007. "Behavior of CFRP Strengthened Reinforced Concrete Beams in Corrosive Environment." *Journal of Composites for Construction*, 11 (3): 291–298. American Society of Civil Engineers (ASCE). https://doi.org/10.1061/(ASCE)1090-0268(2007)11:3(291)/ASSET/569BA605-771D-4480-8479-C2DE01321F9B/ASSETS/IMAGES/13.JPG.

Sun, Y., and G. Qiao. 2019. "Influence of constant current accelerated corrosion on the bond properties of reinforced concrete." *Int J Electrochem Sci*, 14 (5): 4580–4594. Electrochemical Science Group. https://doi.org/10.20964/2019.05.36.

Tapan, M., and R. S. Aboutaha. 2011. “Effect of steel corrosion and loss of concrete cover on strength of deteriorated RC columns.” *Constr Build Mater*, 25 (5): 2596–2603. https://doi.org/10.1016/j.conbuildmat.2010.12.003.

Tastani, S. P., and S. J. Pantazopoulou. 2004. “Experimental evaluation of FRP jackets in upgrading RC corroded columns with substandard detailing.” *Eng Struct*, 26 (6): 817–829. https://doi.org/10.1016/j.engstruct.2004.02.003.

Tazarv, M., and M. S. Saiidi. 2015. “UHPC-filled duct connections for accelerated bridge construction of RC columns in high seismic zones.” *Eng Struct*, 99: 413–422. Elsevier Ltd. https://doi.org/10.1016/j.engstruct.2015.05.018.

Wang, X., S. Wu, J. Jia, H. Li, Y. Wei, K. Zhang, and Y. Bai. 2021. “Experimental evaluation of seismic performance of corroded precast RC bridge columns and the retrofit measure using CFRP jackets.” *Eng Struct*, 245: 112872. Elsevier. https://doi.org/10.1016/J.ENGSTRUCT.2021.112872.

Wang, Z., D. Wang, S. T. Smith, and D. Lu. 2012. “Experimental testing and analytical modeling of CFRP-confined large circular RC columns subjected to cyclic axial compression.” *Eng Struct*, 40: 64–74. Elsevier Ltd. https://doi.org/10.1016/j.engstruct.2012.01.004.

Wright, J. W., and C. P. Pantelides. 2021a. “Axial compression capacity of concrete columns reinforced with corrosion-resistant metallic reinforcement.” *Journal of Infrastructure Preservation and Resilience 2021 2:1*, 2 (1): 1–15. SpringerOpen. https://doi.org/10.1186/S43065-021-00016-3.

Wright, J. W., and C. P. Pantelides. 2021b. “Axial compression capacity of concrete columns reinforced with corrosion-resistant hybrid reinforcement.” *Constr Build Mater*, 302. Elsevier Ltd. https://doi.org/10.1016/J.CONBUILDMAT.2021.124209.

Wu, R. Y., and C. P. Pantelides. 2017. “Rapid repair and replacement of earthquake-damaged concrete columns using plastic hinge relocation.” *Compos Struct*, 180: 467–483. Elsevier Ltd. https://doi.org/10.1016/j.compstruct.2017.08.051.

Yuan, W., A. Guo, W. Yuan, and H. Li. 2018. “Shaking table tests of coastal bridge piers with different levels of corrosion damage caused by chloride penetration.” *Constr Build Mater*, 173: 160–171.

Elsevier Ltd. https://doi.org/10.1016/j.conbuildmat.2018.04.048.

Zhou, A., C. L. Chow, and D. Lau. 2018. “Structural behavior of GFRP reinforced concrete columns under the influence of chloride at casting and service stages.” *Compos B Eng*, 136: 1–9. Elsevier. https://doi.org/10.1016/J.COMPOSITESB.2017.10.011.

Zhou, Y., X. Chen, X. Wang, L. Sui, X. Huang, M. Guo, and B. Hu. 2020. “Seismic performance of large rupture strain FRP retrofitted RC columns with corroded steel reinforcement.” *Eng Struct*, 216. Elsevier Ltd. https://doi.org/10.1016/j.engstruct.2020.110744.

Zhou, Y., B. Zheng, D. Zhao, L. Dang, L. Sui, D. Li, and F. Xing. 2019. “Cyclic bond behaviors between corroded steel bar and concrete under the coupling effects of hoop FRP confinement and sustained loading.” *Compos Struct*, 224. Elsevier Ltd. https://doi.org/10.1016/j.compstruct.2019.110991.